Bacteria Tune a Trade-off between Adhesion and Migration to Colonize Surfaces under Flow

Ahmet Nihat Simsek,[1,2,*] Matthias D. Koch,[3,4,5,*] Joseph E. Sanfilippo,[6] Zemer Gitai,[5] Gerhard Gompper,[1] and Benedikt Sabass[1,2,†]

[1]*Theoretical Physics of Living Matter, Institute of Biological Information Processes, Forschungszentrum Jülich, 52425 Jülich, Germany*
[2]*Department of Veterinary Sciences and Center for NanoScience, Ludwig-Maximilians-Universität München, 80752 Munich, Germany*
[3]*Department of Biology, Texas A&M University, College Station, Texas 77843, USA*
[4]*Lewis-Sigler Institute for Integrative Genomics, Princeton University, Princeton, New Jersey 08544, USA*
[5]*Department of Molecular Biology, Princeton University, Princeton, New Jersey 08544, USA*
[6]*Department of Biochemistry, University of Illinois Urbana-Champaign, Urbana, Illinois 61801, USA*

(Received 22 July 2023; accepted 18 March 2024; published 12 April 2024)

The bacterial colonization of surfaces is a ubiquitous process that shapes nature and profoundly affects human health. While much is known about the biology of this process, the pivotal interplay between physical environment and active bacterial micromechanics remains poorly understood. In fact, strong adhesion and high motility, both of which are essential for surface colonization, are two apparently contradictory goals, as they mutually obstruct each other. Here, we investigate how the human pathogen *Pseudomonas aeruginosa* optimizes its behavior for colonization of surfaces under flow. From the analysis of the dynamics of fluorescently labeled type-IV pili, we construct a mathematical model that quantitatively connects individual motor dynamics with whole-cell motility and migration. The data analysis also reveals that cells upregulate the number of visible pili on surface contact, although individual pili do not display a measurable sensory response to surfaces. When applying shear flow, we unexpectedly find that robust sticking to a surface requires passive surface adhesion rather than pilus activity. Instead, pilus activity actually promotes cell detachment while enabling migration. Using genetic perturbations of the pilus apparatus, it is shown that wild-type cells achieve a trade-off between adhesion and migration by limiting the number of pili. Simulations reveal a generic underlying trait space, where, depending on the interplay of active and passive forces, adhesion and migration are either compatible or a trade-off is required for efficient bacterial surface colonization. The discovered adhesion-migration problem is paradigmatic of a broad class of piliated bacteria and may also have implications for other cells.

DOI: 10.1103/PRXLife.2.023003

I. INTRODUCTION

Most biological processes involving cell migration fundamentally depend on how cells balance static adhesion and migration. Examples include the epithelial mesenchymal transition, cancer metastasis [1,2], immune-cell migration [3], and bacterial infection [4–7]. In the case of bacteria, strong adhesion to surfaces is required for the formation of mechanically robust biofilms. However, surface migration may also be required to explore the environment and to produce dynamic biofilm structures. How can adhesion and migration be optimized simultaneously? We study this generic problem by focusing on the paradigmatic surface migration of *Pseudomonas aeruginosa* [see Fig. 1(a)].

P. aeruginosa is an opportunistic pathogen and the causative agent of various nosocomial infections. Its prominent role as a pathogen is predicated on its ability to colonize a wide variety of environments, including medical catheters, food, and host tissues. *P. aeruginosa* employs dynamic extracellular filaments called type-IVa pili (T4P) to migrate on these surfaces [8–12] [see Fig. 1(b)]. T4P-driven motion is called twitching. The filaments are anchored to a molecular machinery in the cell envelope, where the ATPase PilB drives pilus polymerization, while pilus retraction is driven by the ATPases PilT and PilU [13]. When pili attach to the extracellular environment, retraction generates a pull with measured stall forces around 30 pN and maximum forces around 150 pN [14]. Extracellularly, *P. aeruginosa* T4P attach to most anorganic or organic materials, including glass and hydrogels, with reported bond strengths up to 95 pN [15]. Thus, T4P-driven migration requires sequential attachment, retraction, and detachment of filaments. While the dynamics of freely extending and retracting T4P are well characterized [16], the stochastic interaction of T4P with surfaces during the twitching process is hardly understood.

Pseudomonas is often found in environments where shear forces are present, such as in the urinary tract or in medical tubing (see, e.g., [17–19]). How *P. aeruginosa* adheres to a

*These authors contributed equally to this work.
†b.sabass@fz-juelich.de

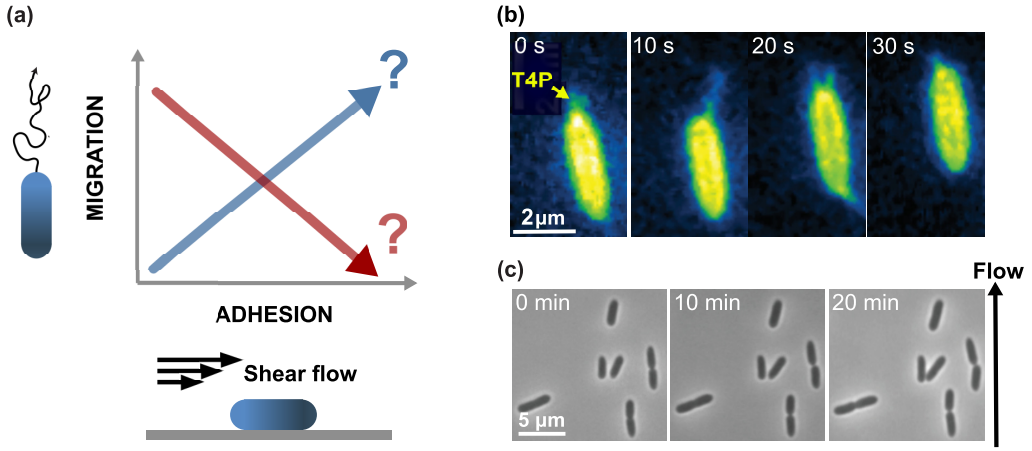

FIG. 1. (a) Migrating cells under mechanical shear have to balance attachment and detachment to remain at the surface. Can cells simultaneously optimize migration and surface adhesion? (b) Live-cell imaging of labeled type-IVa pili (T4P) of *P. aeruginosa* for quantification of extension-retraction dynamics during migration. (c) Δ*pilA* mutants devoid of T4P stick to the surface under shear flow. Fluid shear stress is 1 Pa.

surface under such conditions is a topic of current research. Surface adhesion of bacteria can be quantified by application of hydrodynamic shear forces in micrometer-size flow channels. Such experiments have shown that the surface residence time of *P. aeruginosa* can increase under application of small shear forces [20,21]. For the PA14 strain, flow can also align cells with the T4P pointing upstream, and this orientation results in migration against the flow direction [22]. However, we find that immobile mutants without T4P also stick to surfaces under flow [see Fig. 1(c)]. Such passive surface adhesion of *P. aeruginosa* may depend on various factors that are not yet fully characterized [23]. For the PAO1 strain, exopolysaccharides encoded in the *pel* and *psl* gene clusters contribute to surface adhesion [24–26]. Psl is believed to provide robust cell-surface attachment [27,28], while the additional presence of Pel reportedly results in shorter-range forces that can attach cells tightly to surfaces [29]. Furthermore, adhesion is mediated by other matrix proteins such as CdrA, which is an extracellular adhesin that is coregulated with Pel and Psl. CdrA promotes bacterial aggregation and biofilm formation on surfaces by binding to Psl, but likely also serves as a exopolysaccharide-independent adhesin. Even another class of passive adhesins are Cup fimbriae [30]. However, *cup* genes are described as poorly expressed in the PAO1 strain under standard laboratory conditions [31,32]. Finally, physicochemical forces, such as van der Waals forces and the hydrophobic effect, mediate adhesion to certain substrates [33]. Although passive adhesion mechanisms are clearly central for biofilm formation, their micromechanical role during cell migration remains unclear.

To find out whether bacterial micromechanics are optimized more for migration or for adhesion, we employ fluorescent labeling of T4P in the PAO1 strain [16,34] and quantify the balance of attachment, detachment, and mechanical activity under different conditions. With these new data, we achieve a comprehensive mathematical model that links whole-cell migration to the dynamics of molecular T4P motors. A central discovery is the existence of a complex adhesion-migration trait space where *P. aeruginosa* realizes a trade-off by generating only low numbers of T4P in combination with passive surface adhesion.

II. RESULTS

A. Multiscale model

To derive a model that combines the detailed stochastic dynamics of individual T4P with a cell-wide force balance, we analyze fluorescently labeled T4P for cells on different substrates.

1. Quantification of T4P activity on surfaces

T4P stochastically switch between extension, idle, and retraction states, which is explained by the competitive binding of PilB and PilT to the transmembrane complex [16]. A diagram of T4P states is shown in Fig. 2(a). For adherent cells, the diagram must be extended to include T4P-surface interaction. For this purpose, we compare T4P statistics on substrates with results for bacteria that are held with an optical trap in liquid suspension [see Fig. 2(b)]. Figure 2(c) demonstrates that the pilus lengths obey single-exponential distributions for all conditions. For cells on surfaces, T4P are shorter than for cells that are held in liquid suspension with mean lengths of 0.45 μm and 0.77 μm, respectively [see the inset in Fig. 2(c) and Fig. S4 [35]].

Bacterial colonization depends on the physicochemical properties of the surface (see, e.g., Refs. [36–38]). We therefore ask whether pilus activity depends on extracellular mechanical properties and quantify the T4P statistics on polyacrylamide (PAA) and polyethylene glycol–derived (PEGDMA) hydrogels of different stiffness. Comparison of results for soft and stiff hydrogels, with shear moduli of about 1 kPa and about 55 kPa, respectively, however shows that substrate stiffness is not a systematic major determinant of T4P statistics. While T4P on soft PAA gels are slightly shorter than on rigid PAA gels, a similar dependence on substrate stiffness is not found for PEGDMA gels (see Fig. S4 [35]). Figure 2(d) shows the effect of surface

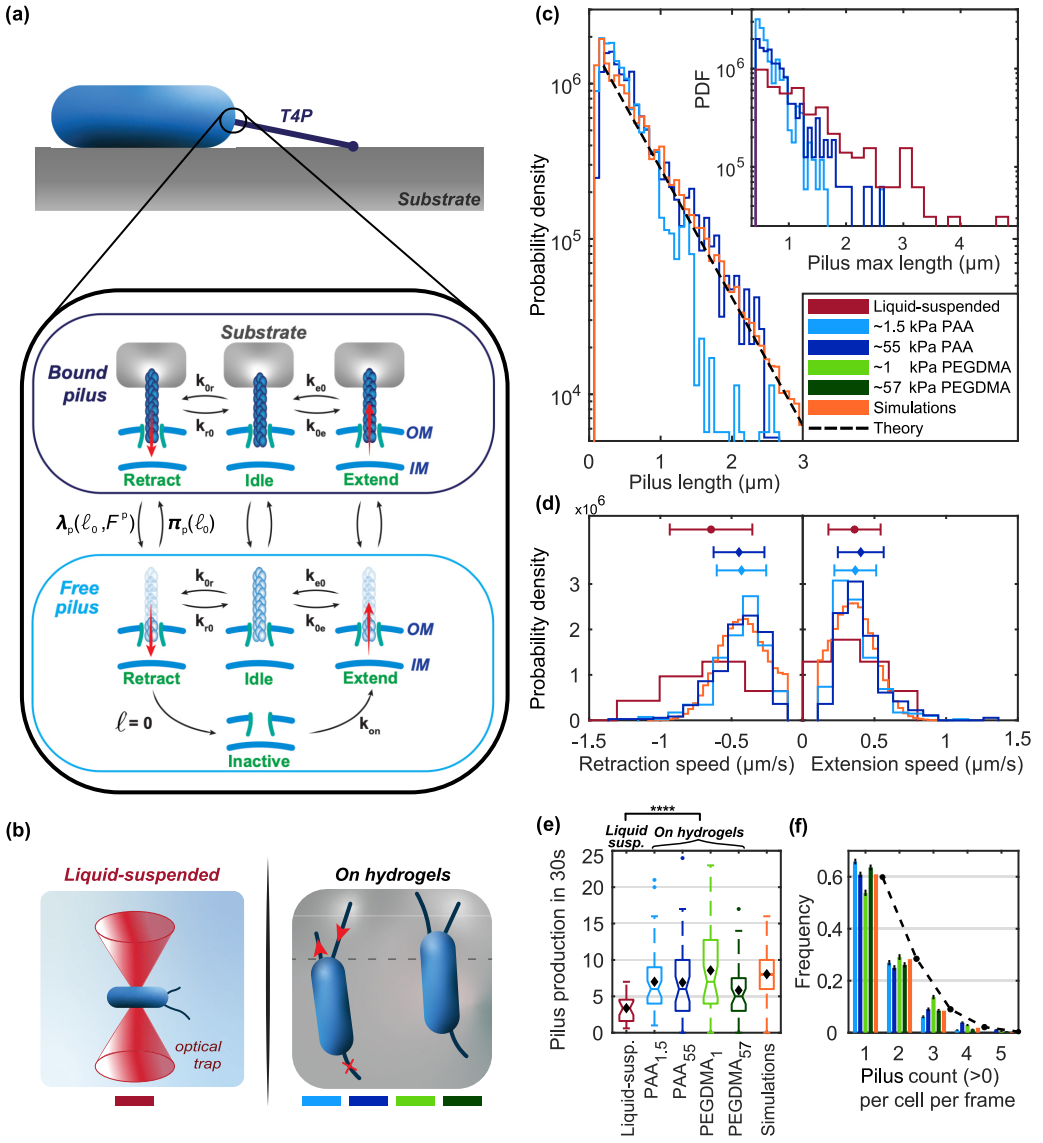

FIG. 2. Systematic construction of a full model for T4P of bacteria on surfaces. (a) State diagram of the stochastic pilus-motor model. Different states describe pili that are bound to the substrate (dark blue) and pili that can extend and retract freely (light blue). Free pili are described by an analytical theory, while simulations generally include bound pili (see Secs. IVE-IVF). (b) Using an optical trap, cells are suspended in liquid for measuring only dynamics of free T4P as in Ref. [16]. Alternatively, the T4P dynamics is quantified for cells lying horizontally on various substrates. (c) T4P length distributions for different substrates. Theory predicts exponential distributions proportional to $e^{-K\ell}$ (see the text for details). The inset shows distributions of maximum length during full extension-retraction cycles. (d) Distribution of average retraction and extension speeds per pilus. Dots and error bars show means and standard deviations, respectively. Simulated speeds are sampled and averaged with time intervals that correspond to the frame rate in experiments. (e) Number of T4P produced in 30 s. Black diamonds mark the means of the data. Cells suspended in liquid produce significantly fewer T4P than cells on surfaces ($p = 3.5\times10^{-9}$, Welch's t-test). (f) Number of simultaneously visible T4P per cell. Only cells with pili are considered. Bars represent standard errors of the means in bootstrapped data. The dashed line shows the Poisson distribution predicted by the theory. Simulation parameters represent T4P on stiff PAA gels ($G' \simeq 55$ kPa). See the Supplemental Material [35] for model details and Table S3 therein for statistics.

interaction on pilus extension and retraction speeds. For cells on hydrogels, the speed distributions do not significantly depend on the type of substrate. However, T4P of cells on hydrogels have a significantly lower mean retraction speed than those of liquid-suspended cells. This finding is consistent with established force-velocity relationships for the T4P machinery, where mechanical loading of bound T4P reduces retraction speed [39].

Cell movement is determined not only by the dynamics of individual T4P but also by their number. We find that, on average, bacteria on all substrates produce about twice as many pili per unit time as bacteria that are held in suspension [see Fig. 2(e)]. This increase of T4P production is consistent with the observation that surface contact correlates with a c-di-GMP-dependent localization of the protein FimW to the cell poles, which in turn promotes T4P production [40].

Furthermore, it has been reported that the transcription of the major pilin gene *pilA* is also repressed for cells in suspension [41]. Figure 2(f) shows the numbers of simultaneously visible T4P per cell, counted for each image frame. For our conditions, *P. aeruginosa* rarely generates more than a single pilus simultaneously. Across hydrogels, no significant difference is found regarding the mean numbers of simultaneously measured T4P per cell. Pilus lifetime, defined as the time between appearance and complete retraction, is not significantly affected by substrate stiffness (see Fig. S4g [35]).

2. Model for free pili

To explain the statistics of T4P, we first construct a model that is represented in the part of the state diagram labeled "Free pilus" in Fig. 2(a) (see Sec. IVE). Pili are assumed to switch between extension (e), idle (0), and retraction (r) states. In this simplified model, pili extend and retract freely; thus, surface interaction is assumed to be rare. Pili are extended and retracted with constant speeds v_e and v_r, respectively. A fully retracted pilus can transition into a hidden inactive state, from which it can reappear stochastically. With these assumptions, we derive explicit formulas for T4P statistics. The resulting distribution for the pilus length ℓ is

$$\mathcal{P}(\ell) = Ce^{-K\ell}, \tag{1}$$

where the transition rate constants depicted in Fig. 2(a) yield a characteristic length $K^{-1} = (k_{0e}v_e v_r + k_{0r}v_e v_r)/(k_{0e}k_{r0}v_e + k_{0r}k_{e0}v_r)$ and C is a normalization constant. The measured pilus length distributions agree with the predicted exponential length distribution [see Fig. 2(c)]. Moreover, the model predicts that the ratio of the probabilities to find an extending or retracting pilus only depends on the ratio of the processes' speeds as $P_e/P_r = -v_r/v_e$. Experimental data confirm this prediction with significance levels of [0.05–0.01] (see Table S1 [35]). Also, the average extension speed correlates with the average retraction speed for individual pili (see Fig. S14 [35]).

For liquid-suspended cells, a fit of the analytical model confirms previously measured values of the rate parameters [16]. However, for cells on substrates, the average T4P are shorter than for liquid-suspended cells [see Fig. 2(c)], which cannot be explained in our model by the slower T4P retraction on surfaces. Based on a parameter variation, we conjecture that the shorter pili on substrates likely result from an increase of the parameter k_{e0}, which determines the rate at which T4P switch from extension to idle. On a molecular level, this finding suggests that the unbinding of the polymerization ATPase PilB is a major determinant of pilus filament length for bacteria on substrates.

The average lifetime of T4P, $\mathcal{T}_{\text{life}}$, determines a timescale during which pili can attach to their environment. We calculate $\mathcal{T}_{\text{life}}$ as mean first-passage time from emergence to complete retraction (see the Supplemental Material [35] and Fig. S6 therein). The theoretical prediction is $\mathcal{T}_{\text{life}} = 2.64$ s, which falls well within the range of lifetimes [2.2–4.0] s that we measure for different substrate conditions. Bootstrap analysis is employed for experimental data to take into account the occurrence of short invisible pili during the finite image-recording intervals (see Fig. S5 [35]). Our linear rate-equation model implies that the number of visible pili per cell must obey a Poisson distribution with a mean $\mathcal{N}_p = k_{\text{on}}\mathcal{T}_{\text{life}}$. This prediction agrees well with the experimental results [see Fig. 2(f)]. Measurement of the exponentially distributed waiting times between the appearance of a new pilus yields $k_{\text{on}} \in [0.25\text{–}0.4]\ \text{s}^{-1}$ (see Fig. S1 [35]).

3. Most pili do not contribute to twitching

How do T4P coordinate extension-retraction dynamics and extracellular attachment to drive twitching migration? Recently, it has been suggested that individual *P. aeruginosa* T4P are able to sense surface contact to initiate retraction [42]. To clarify whether such a mechanism plays a role for our cells, we perform a quantitative analysis of complete cycles of individual T4P-substrate interactions, including extension, surface binding, retraction, and unbinding. Since the unambiguous identification of the surface-binding events is challenging, we focus on the identification of those pili that visually form a mechanical connection with the surface and assume a tensed state during retraction, possibly displacing the bacteria. Pili that form such a surface connection at least once during their lifetime are called contributing pili [see Fig. 3(a) and Sec. IV.C for details regarding the classification].

We find that only 10%–50% of pili actually contribute to twitching [see Fig. 3(b)]. For both PEGDMA and PAA hydrogels, the fraction of contributing pili increases with gel stiffness. This increase of contributing pili can be correlated with smaller hydrogel pore size and hence a higher probability of substrate attachment. Pore sizes for PAA are in the ranges [10–40] nm [43] and [1–5] nm for PEGDMA gels [44]. Note that the pore size of commonly used 0.5% agaraose gels is an order of magnitude larger, in the range of [500–1200] nm [45,46]. Thus, pili are expected to interact less frequently with agarose gels compared to more dense PAA or PEGDMA gels, which explains why T4P filament length statistics are similar for liquid-suspended cells and cells on 0.5% agarose gels [16]. However, chemical substrate properties may also affect the binding rate in principle if the timescale set by diffusive encounter of a pilus binding site is not limiting the process.

Next, we measure the time intervals between defined events in contributing and noncontributing T4P and therewith parametrize our model for T4P-substrate interaction. For example, substrate-binding rate constants are inferred from the average time between the emergence of a new pilus and its first contributing retraction [see Fig. 3(c) herein and Fig. S9 [35]]. We also examine our data regarding the hypothetical surface-contact sensing mechanism suggested in Ref. [42]. The authors of this work measure the delay time between surface contact and retraction of T4P to be [95–215] ms. Such short delay times could result from a mechanism through which T4P are able to sense the surface and then initiate retraction. This mechanism would lead to two predictions for our experimental data, namely, (i) contributing pili should have a shortened mean exploration time, i.e., surface sensing should shorten the mean time during which pili wait in the fully extended state until retraction, and (ii) contributing pili should display a shortened time between pilus genesis and first retraction. Both predictions are not supported by the data.

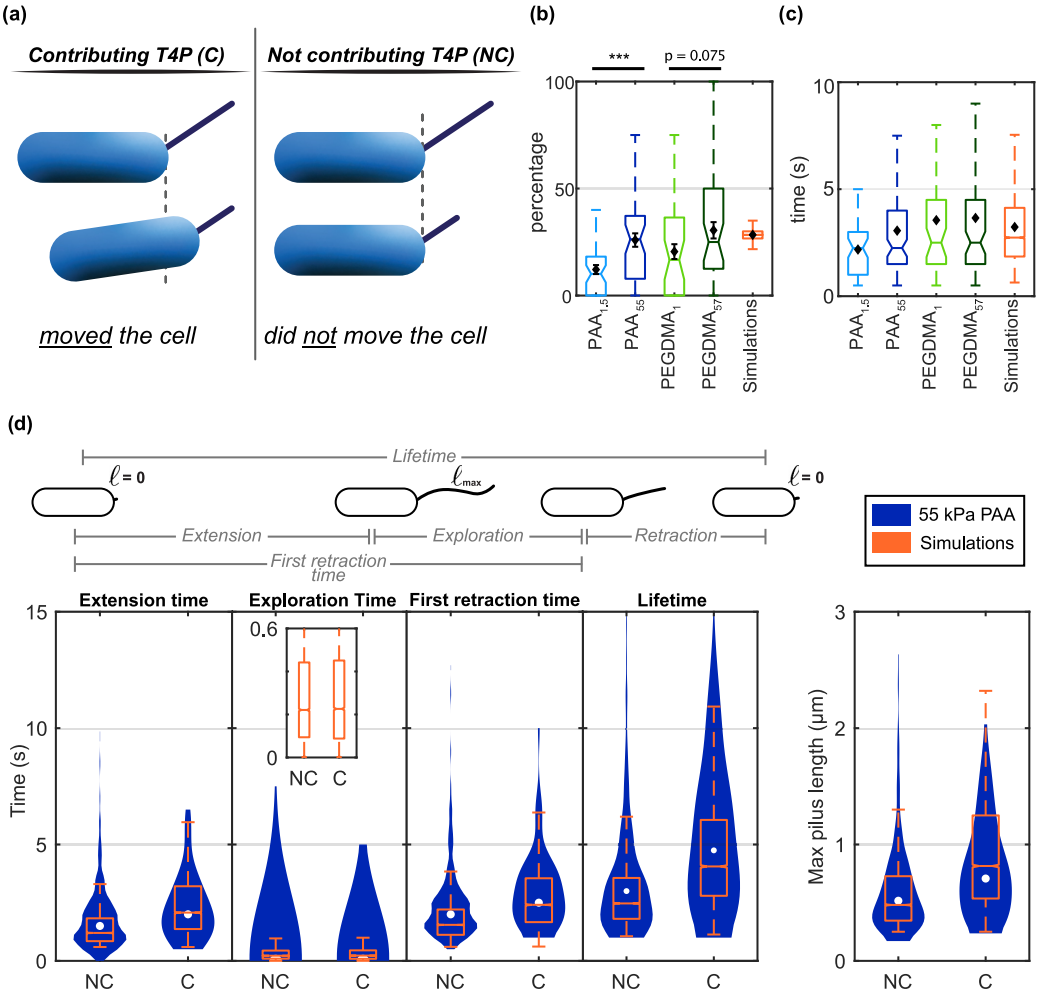

FIG. 3. T4P extension-retraction cycles and surface interaction can be explained without an attachment-dependent retraction trigger. (a) Illustration of T4P categories in our experimental data. Only bound and tense T4P can contribute to twitching. (b) The fraction of contributing T4P per cell is higher on stiffer substrates. The significance of having different medians is $p = 0.000\,44$ on PAA and $p = 0.0753$ on PEGDMA (U test). Error bars show the standard errors of the means. (c) Box plots of the time from creation of a pilus until the first time it is observed to be bound and tensed (contributing). (d) Comparison of the statistics of contributing (C) and noncontributing (NC) pili. Blue violin plots show data from bacteria on 55 kPa PAA, where circles mark the medians. In simulations it is assumed that pili with small length less than 0.25 μm cannot reach the surface. The inset shows enlarged simulation results. See Table S3 [35] for data statistics.

Figure 3(d) shows that the exploration times for contributing and noncontributing pili are distributed similarly with exploration times less than or equal to 0.5 s in more than 80% of the events for all hydrogel conditions. Moreover, contributing pili on average have a larger first retraction time, i.e., start retracting later than noncontributing pili. This finding can be explained by the fact that contributing T4P are more likely to come from a T4P subpopulation that is long lived and therefore more likely to bind to the substrate. For the same reason, contributing pili also spend a longer time on average for extension. In addition, the mean lifetime and length of contributing T4P is greater than that of noncontributing T4P (see Fig. S10 [35]). Using our simulations, we compare resulting average delay times between binding and retraction of T4P with measurements given in Ref. [42]. For consistency with constraints in that experiment, we restrict our analysis only to long pili and also find short delay times on the order of 200 ms without invoking contact sensing since many T4P are already retracting when they bind to the surface. Overall, our experimental data and simulations suggest that the dynamics of individual T4P is governed by random state transitions.

4. *Passive adhesions reduce T4P-driven motion*

Due to the low number of pili per cell, we rarely observe counteracting pili at both ends of bacteria that lead to a tug-of-war, as reported for the bacterium *Neisseria gonorrhoeae* [47,48]. Rather, our time-lapse images suggest that the propulsion of *P. aeruginosa* by T4P retraction is obstructed by apparent cell-substrate forces without any detectable pili being present to hold the cells back. Furthermore, we observe cells that are only slightly displaced by the retraction of T4P at the leading pole and suddenly return to their original position after the pulling T4P detaches from the substrate [see Figs. 4(a) and 4(b)]. These events, which we term snapback, occur on elastic hydrogels. The presence of T4P-independent cell-substrate adhesions is also supported by computer simulations that show that cells with T4P at opposing poles do

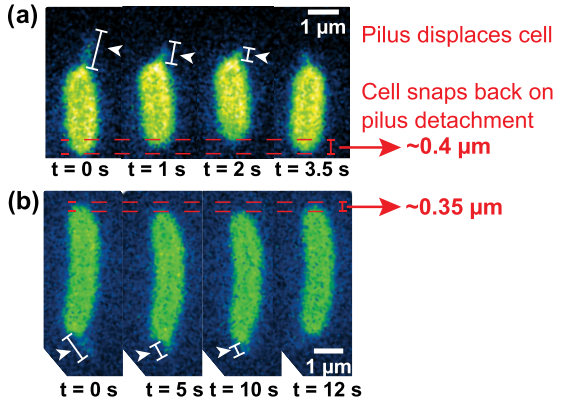

FIG. 4. Snapback events during twitching support the existence of passive adhesive forces between the cell body and the substrate. (a) T4P pulls the cell forward without visible contribution of further T4P at the rear of the cell. Following disengagement of the T4P from the substrate, the cell instantly snaps back to its original position. (b) Further example of a snapback event.

not produce the observed variation in migration dynamics (see Fig. S8 [35]).

B. Twitching migration

1. Two regimes of random motion

Bacterial random walks are characterized by the ensemble-averaged mean-square displacement (MSD) at time τ, denoted by $\Theta(\tau)$ (see the Supplemental Material [35]). For migration of wild-type (WT) cells during short time intervals 1 s $\lesssim \tau \lesssim$ 10 s, we find that the mean-square displacement scales as $\Theta(\tau) \propto \tau^{\alpha}$ with $\alpha \simeq 1$, similar to regular diffusion [see Fig. 5(a)]. For long times, with τ in the range of minutes, we observe superdiffusive motion with $\alpha > 1$, in the range [1.1–1.4] [see Figs. 5(a) and 5(b)]. Similar exponents for the long-time mean-square displacement have been previously reported for *P. aeruginosa* twitching on glass [49,50]. Of course, on very long timescales, diffusive behavior with $\alpha = 1$ is expected due to a complete and random reorientation of the bacteria that is not observable during our finite recording time (see Fig. S3 [35]). The mean-square displacements measured for migration of WT cells on four different hydrogels all show two qualitatively similar regimes, although the magnitudes of the mean-square displacements differ substantially. The observed mean-square displacement can be faithfully reproduced in simulations where the passive surface adhesion is modeled as stochastic bonds with a linearly elastic response. The parameters for passive adhesion bonds depend on the substrate type.

2. Persistent motion on a timescale of minutes

The superdiffusive character of the random walks can be explained by a slow change of the orientation of the bacterial long axis on the measurement timescale, in loose analogy with active Brownian particles. Figure 5(c) illustrates that the autocorrelation of the angle of the long axis decays with a characteristic time on the order of 15 min (see also Fig. S7 [35]). Polar cells, with T4P only at one end, occur in [70–80] % of the data within sliding observation windows of 30 s [see Fig. 5(d) herein and Fig. S2 [35]]. Note that a change of the dominant pole, either spontaneously or through asymmetric division, occurs on timescales larger than 10 min and are therefore not frequently observable in our data. Cell polarity is approximately the same for all substrates and apolar emergence of pili from the long side of the cell body is rare. Simulations show that the experimentally quantified percentage of T4P on one pole is sufficient to explain superdiffusive motion on a timescale of 100 s $\lesssim \tau \lesssim$ 1000 s. Random motion with a persistent character can enable bacteria to follow spatial cues on a surface [41,51].

3. Passive adhesions increase trapping on short timescales and persistence on long timescales

The regime of random motion with $\Theta(\tau) \propto \tau$ found in the experiment for short times is also seen in simulations, where it occurs if passive adhesion forces or counteracting pili transiently hold the cells at one spot. Exemplary snapback events that are caused by the intermittency and varying spatial orientation of pilus-based force generation are shown in Fig. 4. Increasing the passive adhesion strength in the simulations leads to a broadening of the regime with $\alpha \simeq 1$ at short times. Simulations also show that the ratio of contributing pili correlates with the onset of persistent motion on longer timescales, where the higher the ratio of contributing pili, the earlier the onset of persistent motion.

Passive adhesions can also contribute to the persistence of motion by keeping the cell body pointing in one direction. To test experimentally how reduced persistence affects migration, we quantify the mean-square displacement for hyperpilated Δ*pilH* mutants [see Fig. 5(e)], which predominantly adhere to a surface with an upright cell body such that the long axis is oriented approximately normal to the surface. This orientation is likely caused by simultaneous activity of many pili on one pole, which produces a torque that lifts the body upward [49,52]. Upright standing presumably results in low passive adhesive forces since the fraction of the cell body in contact with the surface is reduced. As a result of the reduced persistence, the mean-square displacement characterizing the random walk of Δ*pilH* mutants is well described by a MSD exponent α that is only slightly larger than unity. To accurately capture the random walk of Δ*pilH* mutants in our simulations, random forces that generate Brownian diffusion of a free cell have to be added to the force balance. Such random forces are irrelevant for the migration of wild-type cells which adhere passively to the substrate. Together, experiments and simulations show that passive surface adhesion plays an important role for the migratory behavior of the *P. aeruginosa* wild type. The motion is suggested to be akin to random motion in a rugged potential landscape, where local valleys are explored on short timescales and large excursions occur on long timescales.

C. Surface adhesion under shear flow

1. Twitching reduces surface adhesion under shear

T4P are generally considered to be determinants of cell attachment. However, T4P retraction can also detach cells

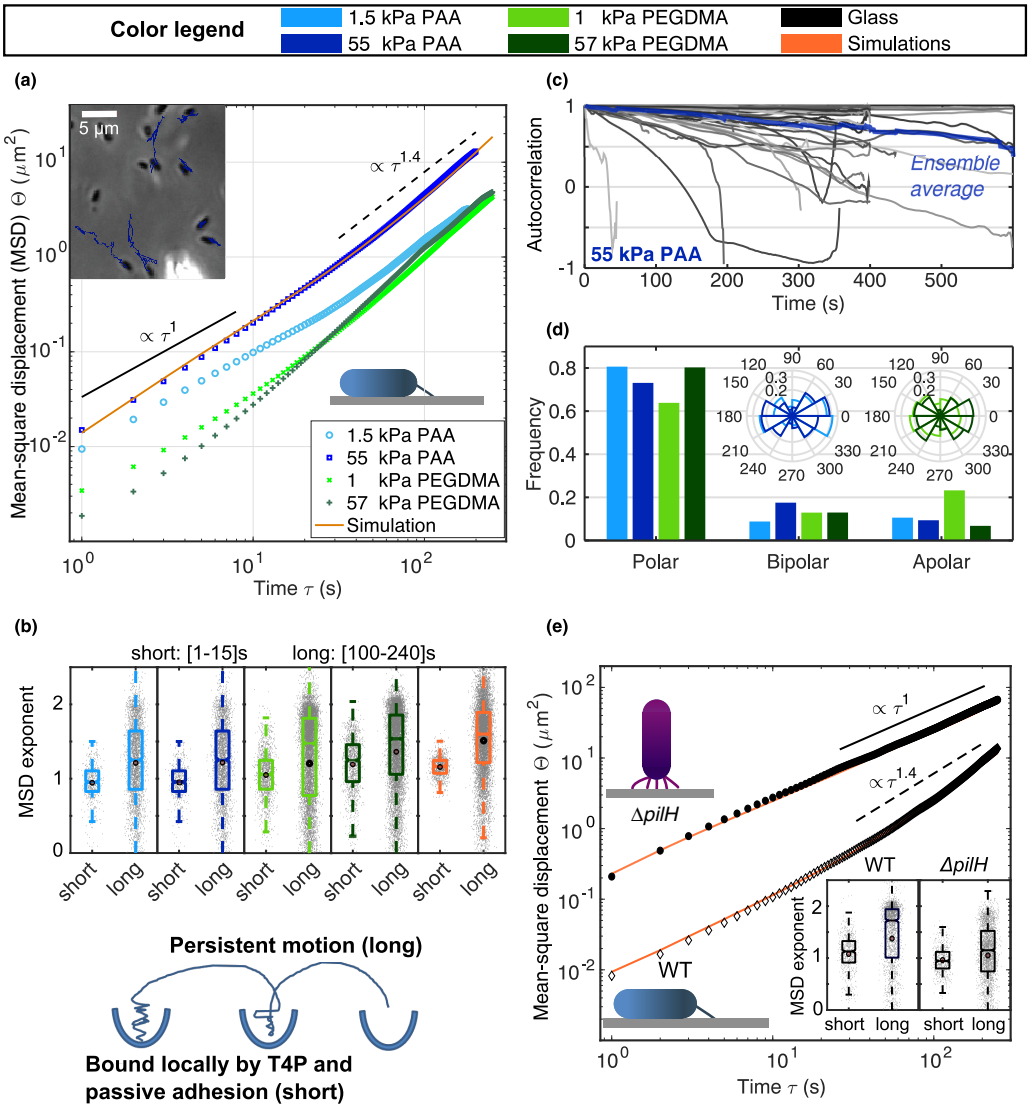

FIG. 5. Pili and passive adhesion together determine two timescales of migration. (a) Ensemble-averaged mean-square displacements (MSDs) of wild-type (WT) cells on different substrates. (b) Exponents of MSDs are different on short and long timescales. Dots show individual measurements. An exponent close to unity on short time intervals can result from random motion of a cell that is locally bound before it explores other areas with persistent motion on longer timescales. (c) Directional autocorrelation of cellular long axis decays over several minutes (see Fig. S7 [35] for the data regarding other gels). (d) Statistics of T4P localization. At any time point, a cell is labeled "Polar" if it has pili only on one pole, "Bipolar" if there are pili on both poles, and "Apolar" if it has pili protruding from the sides of the cell and possibly also from the poles. The inset shows the angular distribution of pili with respect to a long axis of cells that is chosen with random polarity, irrespective of the direction of motion. (e) Ensemble-averaged MSDs of WT cells and Δ*pilH* mutants twitching on glass. Due to their predominantly vertical orientation on the substrate, Δ*pilH* mutants undergo random motion with an exponent that is only slightly larger than unity. Simulation parameters for passive adhesion bonds depend on substrate and cell type and are adjusted to fit MSDs (see the Supplemental Material [35]). Symbols represent the means and error bars are standard deviations of the data.

from the surface and it is therefore unclear whether twitching reduces or increases the residence time of bacteria under shear flow. To answer this question, we perform shear-flow experiments using a microfluidic setup and record cell detachments for different flow rates [see Fig. 6(a)]. Figure 6(c) shows data for pilated wild-type cells that are classified as twitching and nontwitching. Both groups have T4P visible in the fluorescence channel and the average number of T4P per cell is slightly higher for twitching cells ($p = 0.048$ two-sample t-test), 1.27 ± 0.077 for twitching and 0.99 ± 0.117 for nontwitching cells. For all applied flow rates, we find that the ratio of detached cells after 20 min is higher for the twitching bacteria. Thus, cell motion caused by T4P activity correlates with reduced surface adhesion in our experiments.

2. *Passive adhesions are essential for surface adhesion under shear*

To further clarify the role of T4P for surface adhesion under flow, we compare results for wild-type cells with mutants without T4P (Δ*pilA*) and hyperpilated cells (Δ*pilH*) [see Figs. 6(b) and 6(d)]. Typical shear stresses encountered by a

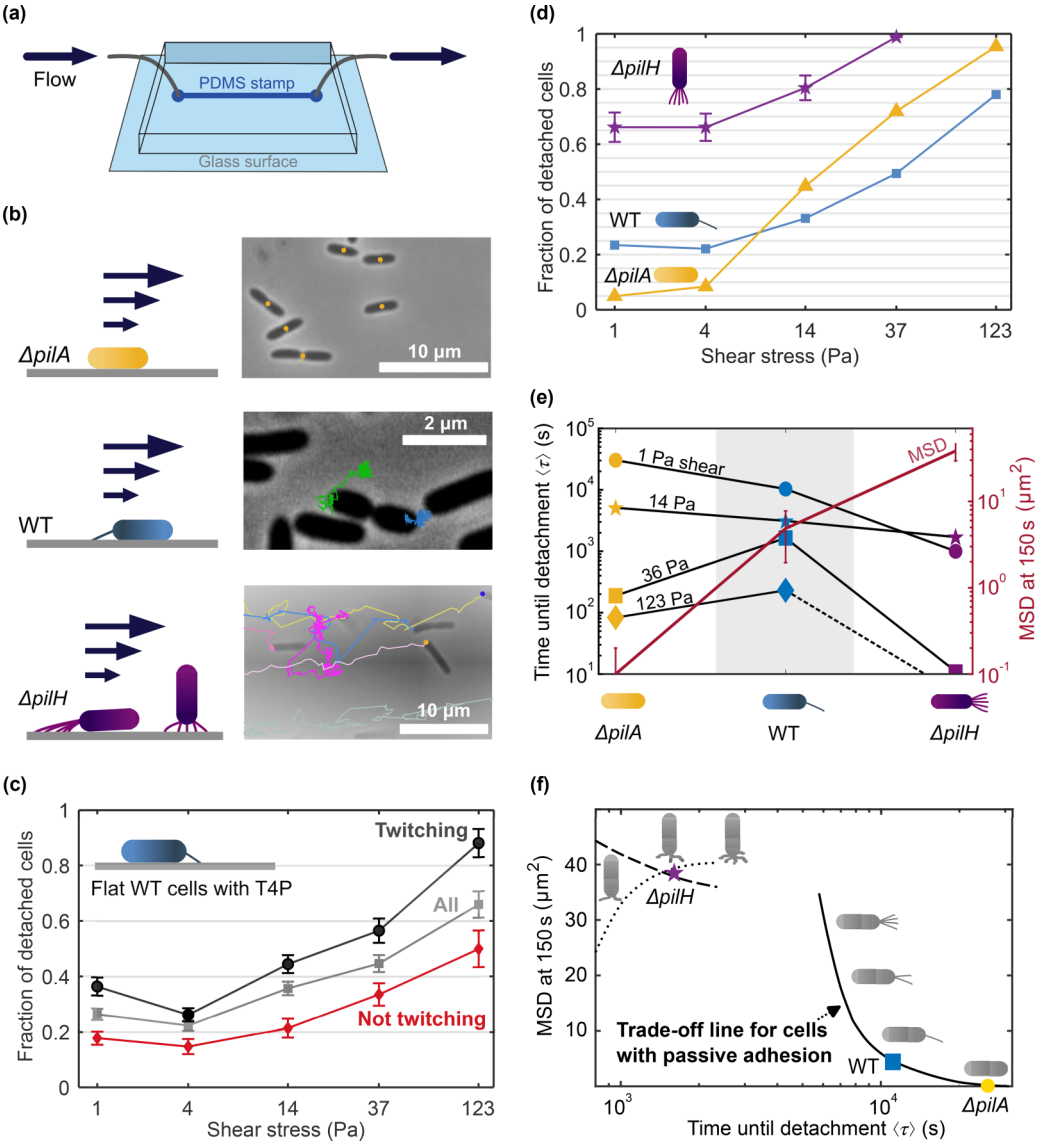

FIG. 6. Trade-off between surface adhesion and migration of *P. aeruginosa*. (a) Setup for shear-flow experiments. (b) Sample trajectories of bacteria under a shear flow that exerts a stress of approximately 1 Pa. The three bacterial strains have different numbers of T4P. (c) Fraction of flat, adhering wild-type cells with T4P that detach under flow in 20 min. The T4P are imaged prior to the onset of flow. Error bars show the standard errors of the means. (d) Fraction of detached cells after 20 min under flow. Detachment is quantified by counting the number of cells every minute over the whole observation time. For the WT and Δ*pilA* strains, standard errors of the mean factions are smaller than symbols in the plot. (e) The average time until surface detachment $\langle\tau\rangle$ and the MSD show opposite trends when the number of pili increases from Δ*pilA* to Δ*pilH* mutants. The WT cells neither adhere best nor migrate best in weak shear, but achieve a trade-off that allows them to optimally combine both properties. The MSD values are recorded in the absence of flow and error bars show 95% confidence intervals. Error bars for $\langle\tau\rangle$ are smaller than the symbols. (f) Qualitative performance diagram for cells that generate different numbers of pili. Passive adhesion enforces a trade-off between adhesion and migration. For upright walking cells, a simultaneous increase of MSD and detachment time may be possible for low noise and weak attachment. The number of pili is varied in simulations by changing the rate constant for pilus generation. Cell detachment is simulated for shear flow of 4 Pa and the MSD is recorded without flow. The solid line shows results for flat cells with passive adhesion, the dashed line upright cells with noise enhancing cell diffusion, and the dotted line upright cells at low noise.

bacterial pathogen in the human host range from the order of 0.01 Pa in the proximal renal tubule [53] to the order of 10 Pa in vascular beds [54]. At these low shear stresses, the smallest fraction of detached cells is achieved by the Δ*pilA* mutant, which can only adhere passively. In contrast, Δ*pilH* cells which have many T4P are most easily detached. This result suggest that passive adhesion forces that anchor cells to a surface are by themselves more effective than T4P in preventing detachment under low shear stress.

For high shear stress above around 14 Pa, the lowest fraction of detached cells is achieved by the wild type. Thus, having a few pili in addition to passive adhesion is the best way to stick under high shear conditions [see Fig. 6(d)]. We suggest that the advantage of pilated cells under high

shear results from a tightened horizontal alignment of the cell body with the surface, which promotes efficient engagement of passive adhesion mechanisms (see Ref. [21]). Since pilated wild-type cells attach to the surface via one pole, hydrodynamic torque tends to align the cell body with the surface while torque produced by pilus retraction pulls the cells upward. For a shear stress of 14 Pa, we estimate the hydrodynamic force that tilts the cells to be about 10 pN, which is comparable to the force magnitude generated by T4P [14]. Therefore, such shear stresses can be sufficient to maintain the cell body close to the substrate.

3. Adhesion-migration trade-off

To understand how *P. aeruginosa* combines surface attachment with migratory exploration, we compare the mean time until detachment under shear flow with the cells' mean-square displacement absence of flow [see Fig. 6(e) herein and Figs. S11–S13 [35]]. The two quantities show an opposite dependence on T4P numbers, where the time until detachment decreases as $\Delta pilH \rightarrow \mathrm{WT} \rightarrow \Delta pilA$ and the mean-square displacement increases as $\Delta pilA \rightarrow \mathrm{WT} \rightarrow \Delta pilH$. The crossing of the curves illustrates that wild-type cells combine the advantage of mutants having no T4P (good surface attachment, poor migration) and of mutants having many T4P (poor surface attachment, good migration).

Optimization can be visualized in a trait-performance space by plotting simulation results for detachment times against mean-square displacements [see Fig. 6(f)]. Since cells are found to generate more T4P on surface contact [see Fig. 2(e)], the T4P generation rate is assumed to be a parameter that is controlled by cells, e.g., on the transcriptional level or by regulatory processes in the Pil-Chp system [55,56]. Accordingly, we vary the rate of T4P generation in our model. Detachment times are predicted qualitatively without taking hydrodynamics into account. For cells that adhere passively to the substrate, simulations reveal an inverse relationship between adhesion and migration. Thus, both quantities cannot be optimized simultaneously by wild-type cells and the curve can be interpreted as a Pareto front quantifying the trade-off between two incompatible traits. However, this front is not a continuous line since a high number of T4P leads to an upright cell configuration in experiments. Simulations of cells in upright configuration show that loose attachment and the resulting Brownian-like motion can allow both an increase and a decrease of the mean-square displacement with T4P numbers. Thus, the vertical configuration does not necessarily enforce a trade-off between adhesion and migration. Nevertheless, the experimental results suggest that the behavior of wild-type cells is characterized by points on the trade-off curve on the right side of the discontinuity, perhaps even in the corner of the curve where the variances are large.

III. DISCUSSION

Pili are unique molecular machines that not only drive the motility of many biological active-matter systems [57–59], but also are an important virulence factor determining the severity of bacterial infections [60]. We systematically dissect the stochastic dynamics of T4P when cells interact with surfaces and construct detailed mathematical models for connecting the motor dynamics to migration of *P. aeruginosa*. Motor states, spatial pili organization, and binding events are carefully characterized on the timescale of seconds to minutes. We find that the average number of T4P increases when cells are placed on a surface. Indeed, various mechanosensory processes reportedly allow *P. aeruginosa* to detect the presence of solid surfaces [12,61–65] and transition from the planktonic state to a sessile state [66–68]. However, we do not find evidence for a sensory mechanism on the level of individual T4P that serves to trigger their retraction on surface contact [42]. Unlike for the cytoskeleton of mammalian cells [69], we find no indication that regulation of the bacterial T4P machinery depends on substrate stiffness. For *P. aeruginosa*, we do not observe a tug-of-war between opposing T4P as seen for coccoid, peritrichously piliated *Neisseriae* [48], where sliding (kinetic) substrate friction reportedly affects motion, at least on the level of microcolonies [70]. Instead, our results are consistent with a model where pseudomonads exhibit passive, sticking substrate friction that may result from physicochemical adsorption or from secreted adhesins such as the exopolysaccharides Psl and Pel [27,71,72]. Passive surface adhesion of the cell body reduces T4P-driven motion, traps cells locally on short timescales, and contributes to persistent motion by preventing random reorientation. Under shear flow, *P. aeruginosa* achieves a trade-off between sticking to a surface and fast migration by maintaining a low average number of T4P. The number of T4P is known to depend on a negative-feedback regulation of *pilA* transcription, as well as on the Chp chemosensory system, which includes the histidine kinase ChpA and two response regulators PilG and PilH [40,41,66,67]. Our results show that the production of T4P is upregulated upon surface contact, but apparently only to a level where T4P activity does not abrogate passive surface adhesion. Thus, bacteria gain adhesiveness by sacrificing migration speed.

Trade-offs between conflicting vital requirements are common in biological systems [73]. Examples include accuracy-efficiency [74] and growth-adaptability [75] problems that can be solved at the level of individual cells or populations. The balance of adhesion and migration is a new perspective on the micromechanical design of diverse biological systems across scales, ranging from bacteria and algae to immune cells and even insects.

IV. METHODS

A. Strains, growth conditions, and pilus labeling

Bacterial cells are grown and prepared for imaging as described previously [16]. In brief, the PilA cysteine knock-in mutant *P. aeruginosa pilA*-A86C is grown in liquid lysogeny broth (LB) Miller (Difco) in a floor shaker at 37 °C. For imaging, Alexa488 maleimide dye (Fisher A10254) is suspended at a concentration of 2.5 mg/ml in anhydrous dimethyl sulfoxide and stored −20 °C. A fresh aliquot is used for each experiment to avoid freeze-thaw-induced degradation of pilus labeling efficiency. Overnight grown cells are diluted 1:1000 in a fresh LB medium and grown to mid logarithmic phase (optical density at 600 nm = 0.4). Dye is added 1:100, incubated

for 45 min at 37 °C without shaking in the dark. Prior to the experiments, cells are washed twice in a low-autofluorescence EZ-rich medium (Teknova) using a tabletop centrifuge at 8 krpm for 30 s and resuspended in 20 μl of a fresh EZ-rich medium.

B. Hydrogel preparation

PAA gels [76] and PEGDMA gels [44] are made as described previously and mounted in a perfusion chamber (Warner Instruments). Prior to experiments, round, 40-mm coverslips (Fisherbrand) are methacrylate silanized by submerging plasma cleaned coverslips in 2% 3-(trimethoxysilyl) propylmethacrylate in 95% ethanol for 10 min. Hydrophobic round 12-mm coverslips (Fisherbrand) are prepared by submerging coverslips in Sigmacote (Sigma) for 10 min. All coverslips are subsequently rinsed three times in 100% ethanol and dried upright on Kimwipes. For preparation of gels, either 2% bis-acrylamide (BAA) and 40% polyacrylamide (AA) solutions (Bio-Rad) are diluted to 7.5% AA + 0.05% BAA ($G' \simeq 1.5$ kPa [77]) and 12% AA + 0.6% BAA ($G' \simeq 55$ kPa [77]) or PEGDMA (Mn 750, Sigma 437468) and 1.2M (356 mg/ml) 2-methacryloyloxyethyl phosphorylcholine (MPC) (Sigma 730114) are diluted to 1.1% PEGDMA + 50% MPC ($G' \simeq 1$ kPa [44]) and 6.3% PEGDMA + 50% MPC ($G' \simeq 57$ kPa [44]) in 496.5 μl ddH2O, respectively. These solutions are degassed for 10 min in a vacuum chamber. To initiate polymerization, 2.5 μl of 10% ammonium persulfate (Biorad) and 1 μl tetramethylethylenediamine (Temed, Biorad) are added and gently mixed by pipetting. Hydrogels are then allowed to polymerize between two chemically modified coverslips that were prepared prior to experiments. Next 10 μl of unpolymerized gel is added between both coverslips resulting in an approximately 50-μm-tall gel. Gels are polymerized for 30 min at room temperature, followed by removal of the hydrophobic coverslip. Finally, gels are washed three times and then incubated for 30 min in an EZ-rich medium.

C. Measurement of T4P dynamics on hydrogels

1. Imaging

To prepare experiments, the excess liquid medium is carefully removed from the gel and 20 μl of cell suspension is added. The inlets to the perfusion chamber are filled with an EZ-rich medium and the chamber is subsequently assembled carefully to avoid air bubbles in the system. The chamber is then mounted on a Nikon TiE microscope housed in an environmental chamber at 37 °C. To remove excess cells in the medium and to continuously provide a fresh medium, a slight flow using a flow pump is introduced. Fluorescent pilus images are taken every 0.5 s using a white light LED source (Excelitas), a GFP filter set, a Nikon Plan Apo 60X WI DIC N2 lens, and an Andor Clara CCD camera with a 1.5× zoom. Bright-field images of bacteria on gel are also taken with a 40× objective and the same setup.

2. T4P data acquisition

Prior to analyzing the fluorescence images, duplicate images are employed to construct lookup tables for contrast optimization. Pili are then identified visually by comparing the original and the processed images. Brightness and contrast of the images are adjusted automatically and despeckled by IMAGEJ, and displayed with a lookup table. The tip and the base on the cell membrane are marked and recorded for each pilus, where the expected measurement error is about 1 pixel (0.07 μm). The process is repeated for all bacteria with observable pili. The pili that are idle for the duration of the experiments are excluded from the analysis. For measuring the occurrence of new pili, cells are imaged only for a few minutes before photobleaching occurs. In the case of bacteria on a substrate, pilus production of multiple cells is quantified simultaneously. A pilus production event is recorded when a new pilus growing out of the cell body is observed for the first time. The number of pilus production events per observation time is calculated for each cell and then averaged for every group.

The contributing fraction of pili is determined from fluorescence-image sequences of bacteria and pili. For every cell, all observable pili are localized and analyzed as described above. Noncontributing pili fluctuate visibly under the microscope, while pili that bind to the substrate are more stationary, tend to straighten up on retraction, and sometimes visually move the cell. Every pilus for which such a stable tense configuration is visible at least once during its lifetime is labeled contributing. The contributing fraction is the fraction of contributing pili in the pooled data.

3. Cell tracking

Migration of cells is quantified by tracking them in phase-contrast images semiautomatically with the IMAGEJ plugin MICROBEJ [78]. The plugin supports subpixel registration and the magnitude of tracking errors is distributed exponentially with a mean of 0.25 pixel lengths. Automatic cell segmentation and tracking is followed by a careful manual error correction. Cells that are only partially adhered were excluded from the analysis.

D. Flow experiments

1. Flow chamber preparation

Microfluidic devices are made as described previously [79]. Briefly, soft lithography masks are designed in AutoCAD and printed by CAD/Art Services. A mold is then made on a silicon wafer (University Wafer) by spin coating SU-8 photoresist (MicroChem). Microfluidic chips are made by pouring freshly mixed and vacuum degassed polydimethylsiloxane (PDMS) (Sylgard 184, Dow) over the mold. The PDMS is cured for 2 h at 60 °C. Individual chips are cut out and bonded to plasma-cleaned 22×40 mm^2 coverslips (Fisherbrand) for 1 h at 60 °C. Each chip has six parallel channels with width $W \simeq 600$ μm, height $H \simeq 110$ or 55 μm, and 2 cm length. Only one channel is used per experiment. The shear stress at the inner channel surface is estimated from the known flow rate as in Ref. [20].

2. Imaging and analysis

Flow experiments are performed on the same microscope as described above using a 100× oil immersion objective and

1.0× zoom. Flow chambers are filled with labeled cells and incubated for 15 min on the microscope at 37 °C prior to starting the experiment. First, pili are imaged every second for 30 s with a maximum flow of 3 μl/min. Second, cells are imaged every 1 s for 20 min in the bright field at flow rates of [25, 75, 250, 750, 2500] μl/min for 55-μm-high channels with WT cells and [100, 300, 1000, 3000, 10 000] μl/min for 110-μm-high channels with mutants. Due to the volume limit of the syringe pump, cells in the largest flow at stresses of 123 Pa could only be recorded for about 10 min. Cell detachment is quantified by counting the number of cells in every frame of a movie. Then stretched exponential functions are fitted to the remaining fraction of cells [20]. Note that the resulting detachment statistics ignore diverse cell behaviors inside the field of view, such as sliding of the Δ*pilA* mutants along with the flow and random jumps of the Δ*pilH* mutants.

E. Analytical model for free pili

The reduced model that is depicted in the inset labeled "Free pilus" in Fig. 2(a) describes the evolution of probability distributions $P_{\dots}(\ell, t)$ for finding a pilus with length ℓ at time t in different states. Visible pili can be extending (e), idle (0), or retracting (r). Once a pilus is fully retracted, the machinery switches to an inactive state. The probability distributions for the length of visible pili $P_{\dots}(\ell, t)$ have units of length^{-1}. The probability to be in a fully retracted inactive state P_{inactv} is unitless. The governing equations read

$$\dot{P}_0(\ell,t) = k_{r0}P_r(\ell,t) + k_{e0}P_e(\ell,t) - (k_{0r} + k_{0e})P_0(\ell,t), \tag{2}$$

$$\dot{P}_e(\ell,t) = k_{0e}P_0(\ell,t) - k_{e0}P_e(\ell,t) - v_e\partial_\ell P_e(\ell,t), \tag{3}$$

$$\dot{P}_r(\ell,t) = k_{0r}P_0(\ell,t) - k_{r0}P_r(\ell,t) - v_r\partial_\ell P_r(\ell,t), \tag{4}$$

$$\dot{P}_{\text{inactv}}(t) = -k_{\text{on}}P_{\text{inactv}}(t) - v_r P_r(\ell,t)|_{\ell=0}, \tag{5}$$

where the time derivatives $\dot{P}_{\dots}$ are set identically to zero since we only require the steady-state solutions $P_{\dots}(\ell)$. No experimental data are available for invisible pili of zero length and we therefore assume in Eq. (5) that a fully retracted pilus instantaneously switches to the inactive state. Using Kramers' method for mean first-passage times, the average T4P lifetime results as $\mathcal{T}_{\text{life}} = \int_0^\infty [P_e(\ell) + P_r(\ell) + P_0(\ell)]d\ell / \lim_{\ell\to 0} v_e P_e(\ell)$. The number of T4P per cell, $\mathcal{N}_p$, obeys a production-degradation subprocess as $\dot{\mathcal{N}}_p(t) = k_{\text{on}} - \mathcal{N}_p(t)/\mathcal{T}_{\text{life}}$. (See the Supplemental Material [35], Sec. 2, for details.)

F. Simulation model for twitching cells

Cells are modelled as pointlike particles having several T4P and passive adhesion bonds. The equation of motion for the cell position $\mathbf{x}$ in a Cartesian two-dimensional system at time t reads

$$\eta\dot{\mathbf{x}}(t) = \sum_{j\in\mathcal{A}_{\text{p}}} \mathbf{F}^{\text{p}}_j + \sum_{k\in\mathcal{A}_{\text{pa}}} \mathbf{F}^{\text{pa}}_k + \mathbf{F}_{\text{shear}}, \tag{6}$$

where $\mathbf{F}^{\text{p}}_j$ is the tensional force exerted by the jth attached T4P ($j \in \mathcal{A}_{\text{p}}$), $\mathbf{F}^{\text{pa}}_k$ is the force transmitted by the kth attached passive adhesion ($k \in \mathcal{A}_{\text{pa}}$), $\mathbf{F}_{\text{shear}}$ is the hydrodynamic shear force, and η is a friction constant. To avoid a modeling of unknown complex hydrodynamics during cell detachment, the time until detachment under shear is taken to be proportional to the mean time until all cell-substrate bonds are broken in the simulations.

The unit vector $\mathbf{e}_j$ denotes the direction of the jth pilus. The force transmitted by this pilus is given by $\mathbf{F}^{\text{p}}_j = \kappa_p \max[(\ell^j - \ell^j_0), 0]\mathbf{e}_j$, where κ_p is a spring constant, ℓ^j is the actual pilus length, and ℓ^j_0 is the pilus rest length. Due to visible filament buckling, T4P are assumed to transmit only tensional forces. In simulations, a pilus in the extension, idle, or retraction state changes its rest length with speeds $v_e > 0$, $v_0 = 0$, and $v_r(F^{\text{p}}_j) = v_{r0}(1 - F^{\text{p}}_j/F_{\text{stall}})$, respectively, where $v_{r0} < 0$. Pili that are not yet bound by the substrate can independently bind to the substrate with constant rate $\pi_p(\ell^j_0)$, where binding only occurs for rest lengths that obey $\ell^j_0 \geqslant 0.25$ μm. Pilus detachment from the surface occurs with a force-dependent rate $\lambda_{\text{p}}(\mathbf{F}^{\text{p}}_j, \ell^j_0)$ if $\ell^j_0 > 0$ [see Fig. 2(a)]. When a retracting pilus reaches $\ell^j_0 = 0$, the pilus detaches from the substrate and becomes inactive. All inactive pili stochastically switch with constant rate k_{on} to an active extending state. When an active pilus is created, the angle determining its initial orientation vector $\mathbf{e}_j$ is drawn from a distribution to match the experimental data [see Fig. 5(d)]. The direction vectors of attached pili are updated at every simulation time step based on the motion of the bacterium.

Passive adhesins act as elastic anchors holding the bacterium to the surface, to which they bind with rate constant π_{pa}. An attached passive adhesion bond transmits the force $\mathbf{F}^{\text{pa}}_j = \kappa_a s^a_j \mathbf{e}^{\text{pa}}_j$, where s^a_j is its stretch. The orientation of the passive adhesin $\mathbf{e}^{\text{pa}}_j$ is initially taken to be antiparallel to the cell's migration direction and is updated as the cell moves ahead. Dissociation of passive adhesion bonds occurs with force-dependent rates $\lambda_{\text{pa}}(\mathbf{F}^{\text{pa}}_j)$. The number of passive adhesins that can bind to the surface is assumed to be constant. For simulation of Δ*pilH* mutants, the number of passive adhesins is set to zero and an approximately isotropic pilus orientation is assumed. For Δ*pilH* mutants, white Gaussian noise is added to the force balance determining the trajectory of cells when they are not attached to the surface.

ACKNOWLEDGMENTS

B.S. and A.N.S. acknowledge funding from the European Research Council (Grant Agreement No. 852585) and by the German Research Foundation (SPP 2332, SA 2643/3-1). A.N.S. acknowledges support from the International Helmholtz Research School of Biophysics and Soft Matter. This work was supported by Grant No. K22AI151263 from the National Institutes of Health to J.E.S.

M.D.K. and B.S. carried out the experiments. A.N.S. and B.S. analyzed data and conducted theoretical work. All authors contributed to the interpretation of the data and to the manuscript preparation.

[1] M. J. Paszek, N. Zahir, K. R. Johnson, J. N. Lakins, G. I. Rozenberg, A. Gefen, C. A. Reinhart-King, S. S. Margulies, M. Dembo, D. Boettiger, D. A. Hammer, and V. M. Weaver, Tensional homeostasis and the malignant phenotype, Cancer Cell **8**, 241 (2005).

[2] U. S. Schwarz and S. A. Safran, Physics of adherent cells, Rev. Mod. Phys. **85**, 1327 (2013).

[3] E. K. Paluch, I. M. Aspalter, and M. Sixt, Focal adhesion-independent cell migration, Annu. Rev. Cell Dev. Biol. **32**, 469 (2016).

[4] H. P. Hahn, The type-4 pilus is the major virulence-associated adhesin of *Pseudomonas aeruginosa*—a review, Gene **192**, 99 (1997).

[5] M. A. Croxen and B. B. Finlay, Molecular mechanisms of *Escherichia coli* pathogenicity, Nat. Rev. Microbiol. **8**, 26 (2010).

[6] A. Persat, C. Nadell, M. K. Kim, F. Ingremeau, A. Siryaporn, K. Drescher, N. Wingreen, B. Bassler, Z. Gitai, and H. A. Stone, The mechanical world of bacteria, Cell **161**, 988 (2015).

[7] C. Berne, A. Ducret, G. G. Hardy, and Y. V. Brun, Adhesins involved in attachment to abiotic surfaces by gram-negative bacteria, Microbiol. Spectr. **3**, 1 (2015).

[8] J. M. Skerker and H. C. Berg, Direct observation of extension and retraction of type IV pili, Proc. Natl. Acad. Sci. USA **98**, 6901 (2001).

[9] J. S. Mattick, Type IV pili and twitching motility, Annu. Rev. Microbiol. **56**, 289 (2002).

[10] V. Pelicic, Type IV pili: *e pluribus unum*?, Mol. Microbiol. **68**, 827 (2008).

[11] L. L. Burrows, *Pseudomonas aeruginosa* twitching motility: type IV pili in action, Annu. Rev. Microbiol. **66**, 493 (2012).

[12] K. Cowles and Z. Gitai, Surface association and the MreB cytoskeleton regulate pilus production, localization and function in Pseudomonas aeruginosa, Mol. Microbiol. **76**, 1411 (2010).

[13] Y.-W. Chang, L. A. Rettberg, A. Treuner-Lange, J. Iwasa, L. Søgaard-Andersen, and G. J. Jensen, Architecture of the type IVa pilus machine, Science **351**, aad2001 (2016).

[14] J. Ribbe, A. E. Baker, S. Euler, G. A. O'Toole, and B. Maier, Role of cyclic di-GMP and exopolysaccharide in type IV pilus dynamics, J. Bacteriol. **199**, e00859 (2017).

[15] A. Touhami, M. H. Jericho, J. Boyd, and T. J. Beveridge, Nanoscale characterization and determination of adhesion forces of *Pseudomonas aeruginosa* pili by using atomic force microscopy, J. Bacteriol. **188**, 370 (2006).

[16] M. D. Koch, C. Fei, N. S. Wingreen, J. W. Shaevitz, and Z. Gitai, Competitive binding of independent extension and retraction motors explains the quantitative dynamics of type IV pili, Proc. Natl. Acad. Sci. USA **118**, e2014926118 (2021).

[17] K. Drescher, Y. Shen, B. L. Bassler, and H. A. Stone, Biofilm streamers cause catastrophic disruption of flow with consequences for environmental and medical systems, Proc. Natl. Acad. Sci. USA **110**, 4345 (2013).

[18] E. Secchi, A. Vitale, G. L. Miño, V. Kantsler, L. Eberl, R. Rusconi, and R. Stocker, The effect of flow on swimming bacteria controls the initial colonization of curved surfaces, Nat. Commun. **11**, 2851 (2020).

[19] R. Rusconi and R. Stocker, Microbes in flow, Curr. Opin. Microbiol. **25**, 1 (2015).

[20] S. Lecuyer, R. Rusconi, Y. Shen, A. Forsyth, H. Vlamakis, R. Kolter, and H. A. Stone, Shear stress increases the residence time of adhesion of Pseudomonas aeruginosa, Biophys. J. **100**, 341 (2011).

[21] J.-J. S. Palalay, A. N. Simsek, J. L. Reed, M. D. Koch, B. Sabass, and J. E. Sanfilippo, Shear force enhances adhesion of *Pseudomonas aeruginosa* by counteracting pilus-driven surface departure, Proc. Natl. Acad. Sci. USA **120**, e2307718120 (2023).

[22] Y. Shen, A. Siryaporn, S. Lecuyer, Z. Gitai, and H. A. Stone, Flow directs surface-attached bacteria to twitch upstream, Biophys. J. **103**, 146 (2012).

[23] Z. Jiang, T. Nero, S. Mukherjee, R. Olson, and J. Yan, Searching for the secret of stickiness: How biofilms adhere to surfaces, Front. Microbiol. **12**, 686793 (2021).

[24] K. D. Jackson, M. Starkey, S. Kremer, M. R. Parsek, and D. J. Wozniak, Identification of psl, a locus encoding a potential exopolysaccharide that is essential for *Pseudomonas aeruginosa* PAO1 biofilm formation, J. Bacteriol. **186**, 4466 (2004).

[25] L. Friedman and R. Kolter, Two genetic loci produce distinct carbohydrate-rich structural components of the *Pseudomonas aeruginosa* biofilm matrix, J. Bacteriol. **186**, 4457 (2004).

[26] S. Kasetty, S. Katharios-Lanwermeyer, G. A. O'Toole, and C. D. Nadell, Differential surface competition and biofilm invasion strategies of *Pseudomonas aeruginosa* PA14 and PAO1, J. Bacteriol. **203**, e00265-21 (2021).

[27] K. Zhao, B. S. Tseng, B. Beckerman, F. Jin, M. L. Gibiansky, J. J. Harrison, E. Luijten, M. R. Parsek, and G. C. L. Wong, Psl trails guide exploration and microcolony formation in *Pseudomonas aeruginosa* biofilms, Nature (London) **497**, 388 (2013).

[28] W. T. Kranz, A. Gelimson, K. Zhao, G. C. L. Wong, and R. Golestanian, Effective dynamics of microorganisms that interact with their own trail, Phys. Rev. Lett. **117**, 038101 (2016).

[29] B. J. Cooley, T. W. Thatcher, S. M. Hashmi, G. L'her, H. H. Le, D. A. Hurwitz, D. Provenzano, A. Touhami, and V. D. Gordon, The extracellular polysaccharide Pel makes the attachment of *P. aeruginosa* to surfaces symmetric and short-ranged, Soft Matter **9**, 3871 (2013).

[30] I. Vallet, J. W. Olson, S. Lory, A. Lazdunski, and A. Filloux, The chaperone/usher pathways of *Pseudomonas aeruginosa*: Identification of fimbrial gene clusters (*cup*) and their involvement in biofilm formation, Proc. Natl. Acad. Sci. USA **98**, 6911 (2001).

[31] I. Vallet, S. P. Diggle, R. E. Stacey, M. Cámara, I. Ventre, S. Lory, A. Lazdunski, P. Williams, and A. Filloux, Biofilm formation in *Pseudomonas aeruginosa*: Fimbrial cup gene clusters are controlled by the transcriptional regulator MvaT, J. Bacteriol. **186**, 2880 (2004).

[32] S. Ruer, S. Stender, A. Filloux, and S. De Bentzmann, Assembly of fimbrial structures in *Pseudomonas aeruginosa*: Functionality and specificity of chaperone-usher machineries, J. Bacteriol. **189**, 3547 (2007).

[33] R. J. Doyle, Contribution of the hydrophobic effect to microbial infection, Microbes Infect. **2**, 391 (2000).

[34] C. K. Ellison, J. Kan, R. S. Dillard, D. T. Kysela, A. Ducret, C. Bérne, C. M. Hampton, Z. Ke, E. R. Wright, N. Biais, A. B. Dalia, and Y. V. Brun, Obstruction of pilus retraction stimulates bacterial surface sensing, Science **358**, 535 (2017).

[35] See Supplemental Material at http://link.aps.org/supplemental/10.1103/PRXLife.2.023003 for further details.

[36] R. Zhang, L. Ni, Z. Jin, J. Li, and F. Jin, Bacteria slingshot more on soft surfaces, Nat. Commun. **5**, 5541 (2014).

[37] M.-C. Duvernoy, T. Mora, M. Ardré, V. Croquette, D. Bensimon, C. Quilliet, J.-M. Ghigo, M. Balland, C. Beloin, S. Lecuyer, and N. Desprat, Asymmetric adhesion of rod-shaped bacteria controls microcolony morphogenesis, Nat. Commun. **9**, 1120 (2018).

[38] S. Gomez, L. Bureau, K. John, E.-N. Chêne, D. Débarre, and S. Lecuyer, Substrate stiffness impacts early biofilm formation by modulating *Pseudomonas aeruginosa* twitching motility, eLife **12**, e81112 (2023).

[39] B. Maier, L. Potter, M. So, C. D. Long, H. S. Seifert, and M. P. Sheetz, Single pilus motor forces exceed 100 pN, Proc. Natl. Acad. Sci. USA **99**, 16012 (2002).

[40] B. J. Laventie, M. Sangermani, F. Estermann, P. Manfredi, R. Planes, I. Hug, T. Jaeger, E. Meunier, P. Broz, and U. Jenal, A surface-induced asymmetric program promotes tissue colonization by Pseudomonas aeruginosa, Cell Host Microbe **25**, 140 (2019).

[41] J. J. Bertrand, J. T. West, and J. N. Engel, Genetic analysis of the regulation of type IV pilus function by the Chp chemosensory system of Pseudomonas aeruginosa, J. Bacteriol. **192**, 994 (2010).

[42] L. Talà, A. Fineberg, P. Kukura, and A. Persat, *Pseudomonas aeruginosa* orchestrates twitching motility by sequential control of type IV pili movements, Nat. Microbiol. **4**, 774 (2019).

[43] D. L. Holmes and N. C. Stellwagen, Estimation of polyacrylamide gel pore size from Ferguson plots of normal and anomalously migrating DNA fragments. I. Gels containing 3% *N*, *N*′-methylenebisacrylamide, Electrophoresis **12**, 253 (1991).

[44] W. G. Herrick, T. V. Nguyen, M. Sleiman, S. McRae, T. S. Emrick, and S. R. Peyton, PEG-phosphorylcholine hydrogels as tunable and versatile platforms for mechanobiology, Biomacromolecules **14**, 2294 (2013).

[45] L. Jiang and S. Granick, Real-space, *in situ* maps of hydrogel pores, ACS Nano **11**, 204 (2017).

[46] M. M. Chui, R. J. Phillips, and M. J. McCarthy, Measurement of the porous microstructure of hydrogels by nuclear magnetic resonance, J. Colloid Interface Sci. **174**, 336 (1995).

[47] B. Maier and G. C. L. Wong, How bacteria use type IV pili machinery on surfaces, Trends Microbiol. **23**, 775 (2015).

[48] R. Marathe, C. Meel, N. Schmidt, L. Dewenter, R. Kurre, L. Greune, M. A. Schmidt, M. Mueller, R. Lipowsky, B. Maier, and S. Klumpp, Bacterial twitching motility is coordinated by a two-dimensional tug-of-war with directional memory, Nat. Commun. **5**, 3759 (2014).

[49] J. C. Conrad, M. L. Gibiansky, F. Jin, V. D. Gordon, D. A. Motto, M. A. Mathewson, W. G. Stopka, D. C. Zelasko, J. D. Shrout, and G. C. L. Wong, Flagella and pili-mediated near-surface single-cell motility mechanisms in *P. aeruginosa*, Biophys. J. **100**, 1608 (2011).

[50] L. Ni, S. Yang, R. Zhang, Z. Jin, H. Chen, J. C. Conrad, and F. Jin, Bacteria differently deploy type-IV pili on surfaces to adapt to nutrient availability, npj Biofilms Microbiomes **2**, 15029 (2016).

[51] N. M. Oliveira, K. R. Foster, and W. M. Durham, Single-cell twitching chemotaxis in developing biofilms, Proc. Natl. Acad. Sci. USA **113**, 6532 (2016).

[52] M. L. Gibiansky, J. C. Conrad, F. Jin, V. D. Gordon, D. A. Motto, M. A. Mathewson, W. G. Stopka, D. C. Zelasko, J. D. Shrout, and G. C. L. Wong, Bacteria use type IV pili to walk upright and detach from surfaces, Science **330**, 197 (2010).

[53] M. Essig and G. Friedlander, Tubular shear stress and phenotype of renal proximal tubular cells, J. Am. Soc. Nephrol. **14**, S33 (2003).

[54] P. F. Davies, Flow-mediated endothelial mechanotransduction, Physiol. Rev. **75**, 519 (1995).

[55] N. B. Fulcher, P. M. Holliday, E. Klem, M. J. Cann, and M. C. Wolfgang, The *Pseudomonas aeruginosa* Chp chemosensory system regulates intracellular cAMP levels by modulating adenylate cyclase activity, Mol. Microbiol. **76**, 889 (2010).

[56] Y. F. Inclan, A. Persat, A. Greninger, J. Von Dollen, J. Johnson, N. Krogan, Z. Gitai, and J. N. Engel, A scaffold protein connects type IV pili with the Chp chemosensory system to mediate activation of virulence signaling in Pseudomonas aeruginosa, Mol. Microbiol. **101**, 590 (2016).

[57] M. C. Marchetti, J.-F. Joanny, S. Ramaswamy, T. B. Liverpool, J. Prost, M. Rao, and R. A. Simha, Hydrodynamics of soft active matter, Rev. Mod. Phys. **85**, 1143 (2013).

[58] G. Gompper, R. G. Winkler, T. Speck, A. Solon, C. Nardini, F. Peruani, H. Löwen, R. Golestanian, U. B. Kaupp, L. Alvarez, E. Lauga, W. C. K. Poon, A. Doostmohammadi, J. M. Yeomans, *et al.*, The 2020 motile active matter roadmap, J. Phys.: Condens. Matter **32**, 193001 (2020).

[59] O. J. Meacock, A. Doostmohammadi, K. R. Foster, J. M. Yeomans, and W. M. Durham, Bacteria solve the problem of crowding by moving slowly, Nat. Phys. **17**, 205 (2021).

[60] H. Tang, M. Kays, and A. Prince, Role of *Pseudomonas aeruginosa* pili in acute pulmonary infection, Infect. Immun. **63**, 1278 (1995).

[61] Y. Brill-Karniely, F. Jin, G. Wong, D. Frenkel, and J. Dobnikar, Emergence of complex behavior in pili-based motility in early stages of *P. aeruginosa* surface adaptation, Sci. Rep. **7**, 45467 (2017).

[62] A. Yang, W. S. Tang, T. Si, and J. Tang, Influence of physical effects on the swarming motility of Pseudomonas aeruginosa, Biophys. J. **112**, 1462 (2017).

[63] A. Siryaporn, S. L. Kuchma, G. A. O'Toole, and Z. Gitai, Surface attachment induces Pseudomonas aeruginosa virulence, Proc. Natl. Acad. Sci. USA **111**, 16860 (2014).

[64] V. D. Gordon and L. Wang, Bacterial mechanosensing: The force will be with you, always, J. Cell Sci. **132**, jcs227694 (2019).

[65] C. A. Rodesney, B. Roman, N. Dhamani, B. J. Cooley, P. Katira, A. Touhami, and V. D. Gordon, Mechanosensing of shear by Pseudomonas aeruginosa leads to increased levels of the cyclic-di-GMP signal initiating biofilm development, Proc. Natl. Acad. Sci. USA **114**, 5906 (2017).

[66] Y. Luo, K. Zhao, A. E. Baker, S. L. Kuchma, K. A. Coggan, M. C. Wolfgang, G. C. L. Wong, and G. A. O'Toole, A hierarchical cascade of second messengers regulates *Pseudomonas aeruginosa* surface behaviors, mBio **6**, e02456-14 (2015).

[67] A. Persat, F. Yuki, J. N. Engel, H. A. Stone, and Z. Gitai, Type IV pili mechanochemically regulate virulence factors in Pseudomonas aeruginosa, Proc. Natl. Acad. Sci. USA **112**, 7563 (2015).

[68] C. K. Lee, J. de Anda, A. E. Baker, R. R. Bennett, Y. Luo, E. Y. Lee, J. A. Keefe, J. S. Helali, J. Ma, K. Zhao, R. Golestanian, G. A. O'Toole, and G. C. L. Wong, Multigenerational memory

and adaptive adhesion in early bacterial biofilm communities, Proc. Natl. Acad. Sci. USA **115**, 4471 (2018).

[69] B. Geiger, J. P. Spatz, and A. D. Bershadsky, Environmental sensing through focal adhesions, Nat. Rev. Mol. Cell Biol. **10**, 21 (2009).

[70] W. Pönisch, C. A. Weber, and V. Zaburdaev, How bacterial cells and colonies move on solid substrates, Phys. Rev. E **99**, 042419 (2019).

[71] K. M. Colvin, V. D. Gordon, K. Murakami, B. R. Borlee, D. J. Wozniak, G. C. L. Wong, and M. R. Parsek, The Pel polysaccharide can serve a structural and protective role in the biofilm matrix of Pseudomonas aeruginosa, PLoS Pathogens **7**, e1001264 (2011).

[72] A. Ghafoor, I. D. Hay, and B. H. A. Rehm, Role of exopolysaccharides in *Pseudomonas aeruginosa* biofilm formation and architecture, Appl. Environ. Microbiol. **77**, 5238 (2011).

[73] O. Shoval, H. Sheftel, G. Shinar, Y. Hart, O. Ramote, A. Mayo, E. Dekel, K. Kavanagh, and U. Alon, Evolutionary trade-offs, Pareto optimality, and the geometry of phenotype space, Science **336**, 1157 (2012).

[74] G. Lan, P. Sartori, S. Neumann, V. Sourjik, and Y. Tu, The energy–speed–accuracy trade-off in sensory adaptation, Nat. Phys. **8**, 422 (2012).

[75] M. Basan, T. Honda, D. Christodoulou, M. Hörl, Y.-F. Chang, E. Leoncini, A. Mukherjee, H. Okano, B. R. Taylor, J. M. Silverman *et al.*, A universal trade-off between growth and lag in fluctuating environments, Nature (London) **584**, 470 (2020).

[76] B. Sabass, M. D. Koch, G. Liu, H. A. Stone, and J. W. Shaevitz, Force generation by groups of migrating bacteria, Proc. Natl. Acad. Sci. USA **114**, 7266 (2017).

[77] T. Yeung, P. C. Georges, L. A. Flanagan, B. Marg, M. Ortiz, M. Funaki, N. Zahir, W. Ming, V. Weaver, and P. A. Janmey, Effects of substrate stiffness on cell morphology, cytoskeletal structure, and adhesion, Cell Motil. Cytoskel. **60**, 24 (2005).

[78] A. Ducret, E. M. Quardokus, and Y. V. Brun, MicrobeJ, a tool for high throughput bacterial cell detection and quantitative analysis, Nat. Microbiol. **1**, 16077 (2016).

[79] J. E. Sanfilippo, A. Lorestani, M. D. Koch, B. P. Bratton, A. Siryaporn, H. A. Stone, and Z. Gitai, Microfluidic-based transcriptomics reveal force-independent bacterial rheosensing, Nat. Microbiol. **4**, 1274 (2019).